Characterization of Palmprints by Wavelet Signatures via Directional Context Modeling

Lei Zhang and David Zhang

***Abstract*—The palmprint is one of the most reliable physiological characteristics that can be used to distinguish between individuals. Current palmprint-based systems are more user friendly, more cost effective, and require fewer data signatures than traditional fingerprint-based identification systems. The principal lines and wrinkles captured in a low-resolution palmprint image provide more than enough information to uniquely identify an individual. This paper presents a palmprint identification scheme that characterizes a palmprint using a set of statistical signatures. The palmprint is first transformed into the wavelet domain, and the directional context of each wavelet subband is defined and computed in order to collect the predominant coefficients of its principal lines and wrinkles. A set of statistical signatures, which includes gravity center, density, spatial dispersivity and energy, is then defined to characterize the palmprint with the selected directional context values. A classification and identification scheme based on these signatures is subsequently developed. This scheme exploits the features of principal lines and prominent wrinkles sufficiently and achieves satisfactory results. Compared with the line-segments-matching or interesting-points-matching based palmprint verification schemes, the proposed scheme uses a much smaller amount of data signatures. It also provides a convenient classification strategy and more accurate identification.**

***Index Terms*—Biometrics, context modeling, feature extraction, palmprints identification, wavelet transform.**

I. Introduction

BIOMETRICS, a robust technique for personal identification, is becoming more and more popular in an increasingly automated world. Biometric approaches utilize automated techniques for measuring and recognizing the identity of a person with certain physiological characteristics [1]–[3]. These characteristics include fingerprints [9], [10], facial features [15], retina and iris patterns [13], speech patterns [14], hand geometry [11], [12], and palmprints [4]–[8]. Based on the intrinsic features of a human being, biometrics recognition has a unique merit: people may lose their keys or access cards, or forget their passwords or PINs, but biometric "keys" or "passwords" are always available for quick identification. While a good biometric system should be reliable, low cost, user friendly, and require small amounts of data, no single biometric technique has yet met all of these prerequisites.

Fingerprint identification [9], [10] is the most well-known and widespread biometric method. It is very reliable, but fingerprint capturing devices are expensive and the stored data is large. Furthermore, it can be difficult to extract some minutia features from some hands, for example from the hands of manual laborers and elderly people, whose fingers are heavily worn down. In some applications, several other methods may be better than fingerprints, since they require fewer data signatures, are less expensive and less intrusive, and avoid the stigma of fingerprinting, which makes people feel like criminals. In recent years, iris-based verification has been successfully developed [13], but it suffers from the discomfort of iris picture capturing that requires users to put their eyes before a camera. Thus, there is a demand for a new automatic personal identification system.

Recently, some works on palmprint-based personal identification were reported [4]–[8]. Similar to fingerprint and iris verification, the palmprint is one of the most reliable means in personal identification because of its stability and uniqueness. In fact, palmprints have been taken as a human identifier for a long time. Using hand features as a base for identity verification is relatively user-friendly and convenient. Some hand-geometry-based identification systems [12], [13] have also been developed but the hand geometry features are not unique and the systems are less accurate in a large database.

Palmprints-based identifiers are not only user friendly; they use less data amount and can be operated using cheap electronic imaging device. In the palmprint identification system developed by the Biometrics Research Centre, Hong Kong, a CCD camera is used to capture a very low resolution (65 dpi) palmprint image. After processing, a palmprint is stored only by a few bytes of data signatures. Fig. 1 shows a typical palmprint image captured by the system. The black rectangle at the middle left of the image is the palmprint fixture. The palm is the inner surface of the hand between the wrist and the fingers. As illustrated in the figure, the main patterns in a palmprint can be generalized as principal lines, wrinkles and creases.

There are usually three principal lines in a palmprint: the heart line, the head line, and the life line. These lines vary little over time, and their shapes and locations on the palm are the most important physiological features for individual identification. Wrinkles are much thinner than the principal lines and much more irregular. Creases are the relatively detailed features that exist all over the palmprint, just like the ridges do in a fingerprint. Generally speaking, for identification tasks the features of principal lines and wrinkles can be exploited and derived from a low-resolution palmprint image. Although some crease-based palmprint recognition methods [8] have been proposed, they require rather fine resolution imaging and consume a large amount of data. Thus, for personal identification, creases are not as robust and persistent as principal lines.

Manuscript received January 21, 2003; revised August 25, 2003. This paper was recommended by Associate Editor Q. Zhu.

The authors are with the Biometrics Research Centre, Department of Computing, The Hong Kong Polytechnic University, Hung Hum, Kowloon, Hong Kong (e-mail: csdzhang@comp.polyu.edu.hk).

Digital Object Identifier 10.1109/TSMCB.2004.824521

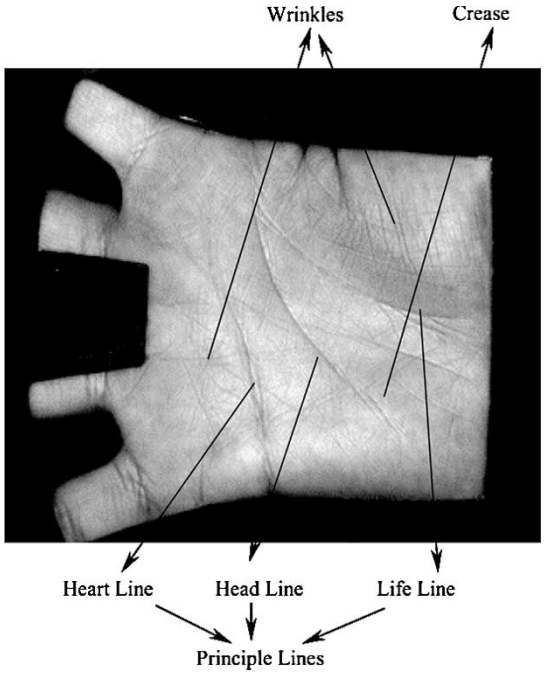

Fig. 1. The main patterns in a palmprint.

Some line-segment-matching and interesting-point-matching based palmprint identification schemes have been presented. The method of Zhang *et al.* [4] first determined some important points and then attempted to extract some line segments for point and line matching. You *et al.* [6] defined some global features for coarse-level verification and locally extracted some interesting points for image matching. The method in [5] is also point-matching based, in which a set of feature points is extracted from the prominent lines and the matching score of the point sets of two palmprints is computed. These schemes are not entirely satisfying in some aspects. First, they are basically off-line schemes in which a palmprint is taken with ink and paper and then scanned by a scanner. The scanning resolution is generally over 100 dpi to ensure the identification accuracy. The second reason for dissatisfaction with these schemes is that they lack an efficient classification strategy. This means that for a given palmprint, it is necessary to search an entire database to find the most similar templates. When searching a sizeable database, this creates a heavy computational burden. The third drawback of these schemes is that they do not characterize palmprints effectively.

The principal lines and wrinkles in a low-resolution palmprint image have provided plenty of information for individual identification. Rather than directly representing and matching them by using some important points and line segments, it would be more efficient to represent these features using statistical signatures. Such signatures will not only precisely record the uniqueness of a palmprint, but also provide better classificatory parameters. Statistical signatures also require less storage space. With the considerations mentioned above, in this paper we develop an approach to characterize the palmprint by a set of statistical signatures for palmprint identification.

Statistical approaches are the most intensively studied and used frameworks in the fields of pattern recognition and feature extraction [26]. These approaches represent patterns by a feature vector of n dimensions. The effectiveness of the method is determined by how well the different patterns can be separated by the representation vector. In the last decades, wavelet-based statistical feature extraction approaches [27]–[32] have been reported with good results. A wavelet transform (WT) [16]–[19] is a time-frequency analysis and it endows the traditional feature extraction methods with a multiresolution and multiscale framework. As the orthogonal wavelet transform (OWT) is translation variant, which is a limitation in texture analysis, in this paper we employ the overcomplete wavelet expansion (OWE), which is translation invariant. No subsampling occurs in the decomposition of OWE and at each scale the wavelet coefficients are of the same size.

A palmprint can be considered as an ordinary gray image to which the traditional statistical feature analysis methods can be applied. However, a palmprint has many particular characteristics that set it apart from an ordinary image. The locations, shapes, and distributions of the principal lines and wrinkles in a palmprint convey redundant information that can uniquely identify a person. In this paper, we will describe how a set of statistical signatures can be derived from these features and used to characterize a palmprint. We decompose the palmprint into several scales by OWE. At each scale and each subband, the predominant coefficients of the principal lines and wrinkles are collected using context modeling. We then define some statistical signatures, which include gravity center, density, spatial dispersivity, and energy, in order to measure the characteristics of the input palmprint. Based on these signatures, we obtain a classification and identification scheme.

This paper is organized as follows. Section II introduces briefly the structure of the employed over-complete wavelet expansion. Section III describes the feature extraction methodology and defines a set of statistical signatures to characterize the palmprints. Section IV describes the identification strategy and gives the experimental results. Section V is the conclusion.

II. OWE

WT represents a function f as a linear combination of elementary atoms or building blocks. A detailed description of the wavelet theory and its relationship with signal processing can be found in Daubechies [16], Mallat *et al.* [17], [18], and Vetterli *et al.* [19]. Denote by $\psi_{m,n}$ the dyadic dilation and translation of a mother wavelet ψ with $m, n \in \mathrm{Z}$

$$\psi_{m,n}(t) = 2^{-m/2}\psi(2^{-m}t - n) \tag{2.1}$$

then f can be written as

$$f = \sum c_{m,n}(f)\psi_{m,n}. \tag{2.2}$$

For orthonormal wavelet bases, there is

$$c_{m,n}(f) = \langle f, \psi_{m,n}\rangle = \int f(t)\psi_{m,n}(t)dt \tag{2.3}$$

where $\langle\cdot,\cdot\rangle$ is the inner product in $L_2(\Re)$. For biorthogonal wavelet bases, we have

$$c_{m,n}(f) = \langle f, \tilde{\psi}_{m,n}\rangle \tag{2.4}$$

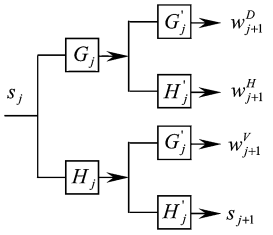

Fig. 2. One-stage decomposition of the 2-D o OWE. Filter $G_j(H_j)$ is interpolated by putting $(2^{j-1}-1)$ zeros between each of the coefficients of $G_0(H_0)$. $G_j'(H_j')$ is the transpose filter of $G_j(H_j)$. w_j^H, w_j^V, and w_j^D are the wavelet coefficients in the horizontal, vertical, and diagonal directions.

where $\tilde{\psi}_{m,n}$ is the dual wavelet of $\psi_{m,n}$. Except for the Haar wavelet, all the compactly supported orthogonal wavelets are not (anti-)symmetrical [16], which is a very important property in signal processing. A compactly supported bi-orthogonal wavelet trades the orthogonality for the symmetric property.

Due to the subsampling in the decomposition process, an OWT is variant with the translation of the input signal. This limits its efficiency in some signal processing applications, such as denoising [24] and texture analysis [30], [31]. The feature extraction scheme presented in this paper is implemented with the OWE, the one-stage decomposition structure of which is shown in Fig. 2. H_j and G_j are the low-pass and high-pass analytic filters. H_j' and G_j' are the transpose filters of them. H_j is interpolated by putting $(2^{j-1}-1)$ zeros between each of the coefficients of H_0, so does for G_j. The output of the OWE is invariant with the translation of the input signal. No subsampling occurs in the decomposition but the analytic and synthetic filters vary at each stage. For OWE, the bandwidth decrease is accomplished by zeros padding of filters instead of subsampling of wavelet coefficients. The high-pass wavelet coefficients of OWE are in three directions: horizontal, vertical, and diagonal at each scale, and they are denoted by w_j^H, w_j^V, and w_j^D. Their size is the same as that of the input image.

In our palmprint-based personal identification system, a palmprint would undergo image acquisition, preprocessing, feature extraction, data signatures storage and classification. After capture by a CCD camera, a palmprint image would be preprocessed to obtain a subimage for feature extraction. The preprocessing procedure can be found in [7]. Preprocessing also eliminates the translation and rotation variances of the acquired palmprint images. The subimage we cut should guarantee preservation of most of the features of the principal lines and wrinkles. After preprocessing, each of the palmprints of different size, translation, and rotation variances is aligned with a comparable area, which is used for feature extraction in subsequent processing.

Fig. 3(a) shows a preprocessed palmprint image, and Fig. 3(b)–(c) shows the two-level OWE of the image. (For visual convenience, the pixels' magnitudes are rescaled.) Fig. 3(b) shows the wavelet coefficients in the three directions at the first scale and (d) shows them at the second scale.

III. Characterization of Palmprint by Wavelet Signatures: The Methodology

Several palmprint-identification methods have previously been proposed which were essentially based on line-segments matching and interesting-point matching. Zhang *et al.* [4] verified an input palmprint by comparing its extracted datum points and line segments with the database. The method in [5] is a complete point-matching process. The scheme of You *et al.* [6] is a half point-matching process. It uses some global features of the palmprint for a coarse-level classification and then uses the extracted interesting points for image matching. These schemes do not characterize palmprints efficiently and completely with the information for individual identification conveyed by the principal lines and wrinkles.

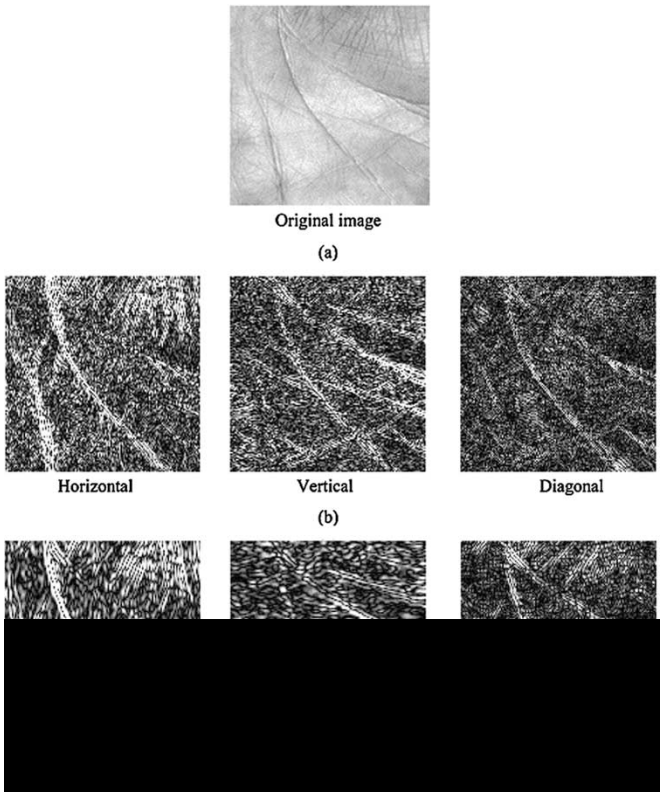

Fig. 3. A preprocessed palmprint image and its OWE at the first two scales. (a) Original palmprint image. (b) Wavelet coefficients in the three directions at the first scale. (c) Wavelet coefficients in the three directions at the second scale.

In this paper, we will record a palmprint by a set of statistical signatures, instead of line segments or interesting points. Statistical approaches have been widely used in the applications of pattern recognition for a long time [26] and wavelet-based statistical feature extraction approaches [27]–[32] have been used with good results, providing the traditional methods with a multiscale framework. Unlike an ordinary image, a palmprint has many particular characteristics, such as the location, shape and distribution of principal lines and wrinkles. These characteristics are important in uniquely identifying a person. In the following sections, a set of wavelet-based statistical signatures will be derived to measure these features of the input palmprint, and, based on these signatures, we subsequently obtain an efficient hierarchical classification and identification scheme.

A. Directional Context Modeling of the Wavelet Coefficients

From Fig. 3, we can see that the principal lines and the thicker wrinkles are enhanced in the wavelet coefficients. Roughly speaking, the horizontal edges are detected in w_j^H, and the vertical and diagonal edges are detected in w_j^V and w_j^D.

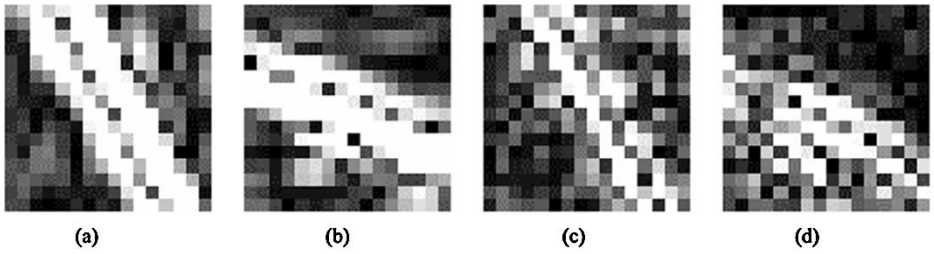

Fig. 4. Zoomed-in images of the edge structures in the three directions of the wavelet coefficients. (a) Horizontal edge structure. (b) Vertical edge structure. (c) Diagonal edge structure in the same position of that in (a). (d) Diagonal structure in the same position of that in (b).

However, the distribution of these edges is rather dispersed. In each subband, it is expected that we could collect the interested edges with similar structures, group the most important horizontally distributed edges in w_j^H, and the vertically and diagonally distributed edges in w_j^V and w_j^D.

The context modeling technique, which was widely used in coding [21], [22] and denoising [20] to differentiate and to gather pixels with some similarities (although not necessarily spatially adjacent), is a good choice for classification. The context value of a given coefficient is defined as a function of its neighbors. The weighted average of its adjacent pixels is often employed. By computing the context of each wavelet coefficient, it is possible to collect the pixels with similar characteristics, whose context values fall into a specified field.

The widths of the principal lines and some heavy wrinkles are much greater than those of other features in a palmprint. Fig. 4(a)–(d) illustrates zoomed-in images of the typical edge structures of the principal lines in horizontal, vertical, and diagonal directions. The edges in Fig. 4(a) are of considerable width across the horizontal pixels, while the edges in Fig. 4(b) possess a sizable width across vertical pixels. The diagonal edges in Fig. 4(c) and (d) are narrower than those in Fig. 5(a) and (b), while they propagate consecutively in the diagonal direction. These properties can be exploited to determine the interesting feature structures in the associated subband.

We denote by $w_j^*(n,m), * = H, V, D$ the coefficient located at the nth row and mth column in wavelet subband w_j^*. It is observed that if a horizontal edge point, which is produced by principal lines or heavy wrinkles, occurs at $w_j^H(n,m)$, its left and right neighborhoods are also likely to be horizontal edge points. Similarly, if a vertical edge point produced by principal lines or heavy wrinkles occurs at $w_j^V(n,m)$, its upside and downside neighborhoods are also likely to be vertical edge points. As for the diagonal edges in subband w_j^D, if the palmprint image is captured from a right hand, the diagonal edge directions of the principal lines are basically along $-\pi/4$; if the palmprint is of a left hand, the diagonal edges produced by the principal lines are basically along $\pi/4$. We then define the directional context of w_j^*, and identify the interested edges by their context values.

Referring to Fig. 5(a)–(d), for each wavelet coefficient $w_j^*(n,m)$ in a subband, denote by $w^*_{j,(n,m)}(1)$–$w^*_{j,(n,m)}(4)$ the absolute values of its neighborhood four elements. Define

$$\vec{u}^*_{j,(n,m)} = \left[w^*_{j,(n,m)}(1) \quad \cdots \quad w^*_{j,(n,m)}(4) \quad |w^*_{j+1}(n,m)| \right] \tag{3.1}$$

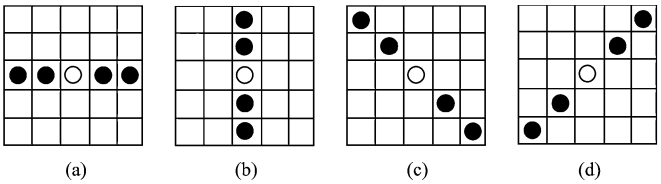

Fig. 5. The employed four neighborhoods (black points) in the calculation of the directional context values. (a) Horizontal direction. (b) Vertical direction. (c) Diagonal direction for right-hand palmprint. (d) Diagonal direction for left hand palmprint.

as the associated vector of $w_j^*(n,m)$. The absolute values rather than the original values are used in the context calculation because the orthogonal wavelet coefficients are weakly correlated, but the absolute values of neighboring coefficients are correlated [25]. Thus, the average of absolute values would yield more meaningful information than the original values. The parent coefficient $w^*_{j+1}(n,m)$ at the adjacent coarse scale is also introduced in the vector $\vec{u}^*_{j,(n,m)}$ since the wavelet coefficient dependencies do not only exist within each scale, but also between scales [23]. If $w_j^*(n,m)$ is a significant coefficient at a scale, its parent coefficients at the coarser scales are much likely to be significant too.

Similar to the context definition used in coding [21], [22] and denoising [20], the directional context value of $w_j^*(n,m)$ is defined here as the weighted average of its associated vector $\vec{u}^*_{j,(n,m)}$

$$c_j^*(m,n) = \vec{u}^*_{j,(n,m)} \vec{h}^*_j \tag{3.2}$$

where $\vec{h}^*_j$ is a 5×1 weighted vector. It should be noted that because the absolute values of the wavelet coefficients are used in $\vec{u}^*_{j,(n,m)}$, the context values are mostly positive. To determine the weighted vector $\vec{h}^*_j$, the least-square estimate is used. $c_j^*(m,n)$ is first approximated by the absolute value of $w_j^*(n,m)$ and then the least-square estimation of $\vec{h}^*_j$ is computed by

$$\vec{h}^*_j = ((\vec{U}^*_j)^T \vec{U}^*_j)^{-1} (\vec{U}^*_j)^T |\vec{Y}^*_j| \tag{3.3}$$

where

$$\vec{U}^*_j = \begin{bmatrix} \vec{u}^*_{j,(1,1)} \\ \vec{u}^*_{j,(1,2)} \\ \vdots \\ \vec{u}^*_{j,(N,M)} \end{bmatrix} \quad \text{and} \quad \vec{Y}^*_j = \begin{bmatrix} w_j^*(1,1) \\ w_j^*(1,2) \\ \vdots \\ w_j^*(N,M) \end{bmatrix} \tag{3.4}$$

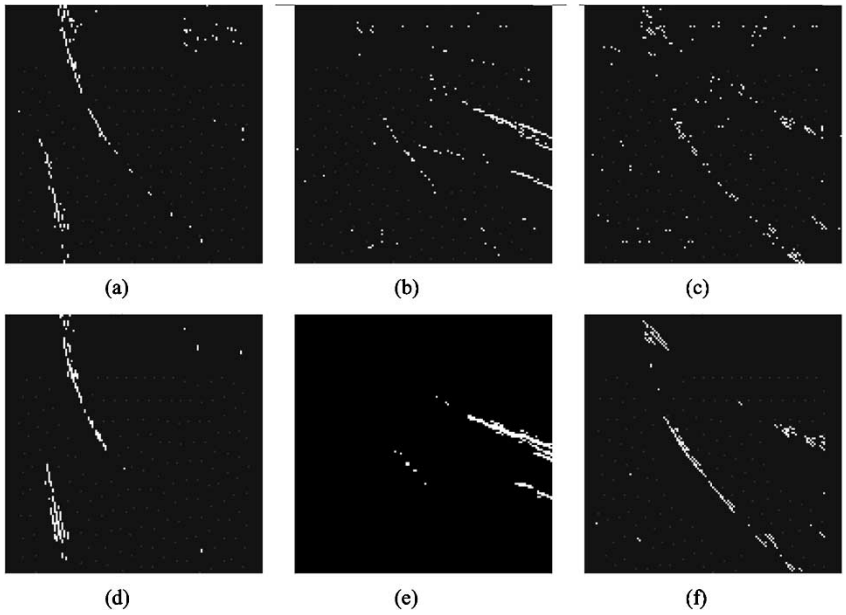

Fig. 6. (a)–(c) The 200 most significant wavelet coefficients in w_1^H, w_1^V, and w_1^D, respectively. (d)–(f) The 200 most significant context coefficients in c_1^H, c_1^V, and c_1^D, respectively. It is seen that by directional context modeling, the edge structures in the corresponding direction are collected much more concentratively and the minor wrinkle features are eliminated.

where N and M are the number of total rows and columns of subband w_j^*. $\overrightarrow{U}_j$ is a $N \cdot M \times 5$ matrix and $\overrightarrow{Y}_j$ is a $N \cdot M$ length column vector.

By using context modeling, the coefficients of similar natures can be well collected. Similar structures have approximate context values, and by sorting the context values c_j^* in ascending order, the wavelet coefficients $w_j^*(n,m)$ could be classified into several groups. Since the interested horizontal edge structures produced by the principal lines or heavy wrinkles have high magnitudes, their directional context values are predominant in c_j^*. We collect the most significant L_j coefficients in c_j^* as the edge points in the associated direction. The edge structures will be enhanced as the scale number increases, the number L_j should be increased proportionally. We set it to be proportional to the scale parameter j

$$L_j = L * j \tag{3.5}$$

where L is a constant preset number.

By the above directional context modeling, the horizontal, vertical, and diagonal edge structures can be more accurately determined than directly thresholding the wavelet coefficients $w_j^*(n,m)$. In Fig. 6(a)–(c), the most significant 200 points of the wavelet subband w_1^H, w_1^V, and w_1^D in Fig. 3(b) are shown respectively, and the greatest 200 coefficients in the corresponding context matrix c_1^H, c_1^V, and c_1^D are illustrated in Fig. 6(d)–(f) respectively. Obviously, the edges in Fig. 6(d)–(f) are more concentrated around the principal lines, while the edges in Fig. 6(a)–(c) are a little more dispersed. Too much information on minor wrinkle features is preserved in Fig. 6(a)–(c) while being eliminated in Fig. 6(d)–(f).

B. Characterizing the Palmprint Using Context-Based Wavelet Signatures

Various wavelet signatures have been proposed in [27]–[32], and the popularly used ones are energy, histogram, and co-occurrence signatures. As for palmprint identification, these signatures neither completely exploit the existed features nor sufficiently characterize the palmprints. In this section, we will define a set of context-based statistical signatures to adequately characterize a palmprint.

We denote by t_j^* the L_jth great value in the context value matrix c_j^* of each subband w_j^*,

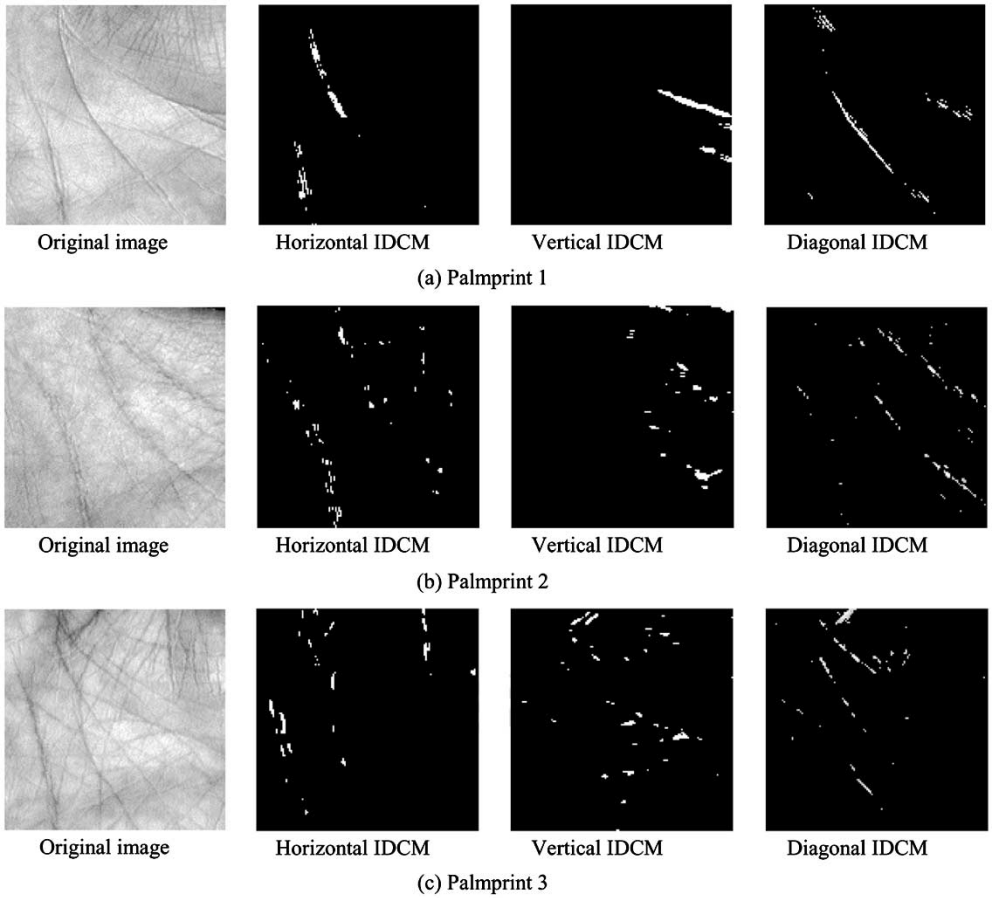

Fig. 7. Some typical palmprint images and their IDCM at the second wavelet scale in the horizontal, vertical, and diagonal directions for (a) palmprint 1, (b) palmprint 2, and (c) palmprint 3.

the gravity centers of $\bar{c}_j^*$ are of close values along different scales with some variations. The signature of the average gravity center (SAGV) of a IDCM $\bar{c}_j^*$, denoted by $(\bar{x}^*, \bar{y}^*)$, is defined as the mean of gravity center sequences $(x_1^* \ \cdots \ x_J^*)$ and $(y_1^* \ \cdots \ y_J^*)$

$$\begin{cases} \bar{x}^* = \dfrac{1}{J}\displaystyle\sum_{j=1}^{J} x_j^* \\ \bar{y}^* = \dfrac{1}{J}\displaystyle\sum_{j=1}^{J} y_j^* \end{cases} \tag{3.9}$$

where J is the total number of wavelet decomposition level.

2) The Density Signature: In the palmprints with deep, concentrative principal lines and weak wrinkles (for example, the first palmprint in Fig. 7), the points in the associated IDCMs are mostly concentrated around the principal lines. In the palmprints with shallow, sparse principal lines and relatively strong wrinkles, the points in the associated IDCMs are more sparsely distributed. Fig. 7 shows that, intuitively, the IDCM of the first palmprint is more compact, and the IDCMs of the other palmprints are looser.

A signature of density (SD) of an IDCM could be defined to characterize the above-mentioned feature of a palmprint. For the ith nonzero coefficient in $\bar{c}_j^*$, denote it as $\bar{c}_j^*(i)$, and let $\Lambda_{j,(i)}^*$ be a square window centered at $\bar{c}_j^*(i)$ and with a proper size l. Denote by $K_{j,(i)}^*$ the number of nonzero points in $\Lambda_{j,(i)}^*$, and then the SD of IDCM $\bar{c}_j^*$ is defined as

$$D_j^* = \frac{1}{L_j}\sum_{i=1}^{L_j} K_{j,(i)}^*. \tag{3.10}$$

The density signature is proportional to the compactness of the point in the IDCM. For example, suppose l to be 5, the values of D_1^* of the first palmprint in Fig. 7 are calculated to be 8, 10, and 6, respectively, in the horizontal, vertical, and diagonal directions. Those of the second palmprint are 5.7, 6, and 3, respectively.

3) The Spatial Dispersivity Signature: The SD defined in Section III-B-2 measures the compactness of the points in an IDCM, but it does not exploit the spatial distribution of the points. From Fig. 7, we can see that although the last two IDCMs are both similarly compact, they are very different in the spatial distribution of their points.

The heart line of a typical palmprint is vertical while the life line is horizontal, and the head line is diagonal. This is also well reflected in the IDCMs. Referring to Fig. 7, suppose we project the vertical IDCM of the first palmprint into y-coordinate, it can be imagined that the resulted projection will concentrate mainly in two local areas. But it can be imagined that if the vertical

IDCM of the last palmprint were projected into the y-coordinate, the projection would be more evenly distributed.

We first assign an associated projection vector (APV) to each IDCM. For the horizontal IDCM $\bar{c}_j^H$, which is projected into the x -coordinate, the APV is defined as

$$\vec{p}_j^{\,H}(m) = \sum_{n=1}^{N} \bar{c}_j^H(n,m), \quad m = 1,2,\ldots,M. \tag{3.11}$$

The vertical IDCM $\bar{c}_j^V$ is projected into the y-coordinate, and its APV is defined as

$$\vec{p}_j^{\,V}(n) = \sum_{m=1}^{M} \bar{c}_j^V(n,m), \quad n = 1,2,\ldots,N. \tag{3.12}$$

The diagonal IDCM $\bar{c}_j^D$ should be projected along the direction of $-\pi/4$ for the right hand, and along the direction of $\pi/4$ for the left hand. Here, we consider the right hand and the result of the left hand can be derived similarly. The APV of $\bar{c}_j^D$, denoted by $\vec{p}_j^{\,D}(k)$ will have K elements, where $K = N+M-1$. Suppose $M \geq N$, $\vec{p}_j^{\,D}(k)$ is defined as (the result when $M < N$ can be derived similarly) in (3.13), shown at the bottom of the page. The APV is then normalized as

$$\bar{\vec{p}}_j^{\,*}(k) = \frac{\vec{p}_j^{\,*}(k)}{\sum_i \vec{p}_j^{\,*}(i)}. \tag{3.14}$$

We call $\bar{\vec{p}}_j^{\,*}$ the normalized associated projection vector (NAPV) of $\bar{c}_j^*$. The signature of spatial disperse (SSD) is defined as the reciprocal of the standard deviation of $\bar{\vec{p}}_j^{\,*}$

$$s_j^* = \frac{1}{\sqrt{\frac{1}{I}\sum_{i=1}^{I}(\bar{\vec{p}}_j^{\,*}(i) - \bar{p}_j^*)^2}} \tag{3.15}$$

where

$$\bar{p}_j^* = \frac{1}{I}\sum_{i=1}^{I} \bar{\vec{p}}_j^{\,*}(i) \tag{3.16}$$

is the mean of the NAPV $\bar{\vec{p}}_j^{\,*}$.

The NAPVs $\vec{p}_j^{\,*}$ of the IDCMs $\bar{c}_j^*$ in Fig. 7 are plotted in Fig. 8. Evenness in the distribution of an NAPV can be reflected in the SSD. If an NAPV is very unevenly distributed, its standard deviation will be high and the value of the SSD will be small and vice versa. The SSDs of the three horizontal NAPVs in Fig. 8 are 71.7, 109.3, and 75.5. The SSDs of the the vertical NAPVs are 82.8, 86.0 and 102.8 and the SSDs of the diagonal NAPVs are 100, 110.4, and 131.5.

4) The Energy Signature: The energy signature is one of the most popularly used wavelet signatures. In many publications [27]–[29], [31], the energy signature has been successfully applied to texture classification. Chang *et al.* [27] characterized a class of middle frequency dominated textures only by their energy signatures with a tree-structured wavelet packet transform. In [31], it is shown that better performance can be achieved by combing the wavelet energy signature with the wavelet histogram and the co-occurrence signatures.

Traditionally, the energy signature is defined as the global power of each wavelet subband w_j^*

$$e_j^* = \frac{1}{N \cdot M}\sum_{n=1}^{N}\sum_{m=1}^{M}(w_j^*(n,m))^2. \tag{3.17}$$

Since the wavelet coefficients within each subband are well modeled by the GGD, which is zero mean, the energy signature e_j^* is truly the variance of the wavelet coefficients, and the sequence $\{e_j^*\}_{j=1,2,\ldots,J}$ reflects the distribution of energy along the frequency axis over scales for a fixed direction. However, the energy signature defined above represents the variation of the global palmprint image, but not the structures in which we are interested.

Define

$$\bar{w}_j^*(n,m) = \begin{cases} w_j^*(n,m), & \text{if } c_j^*(n,m) \geq t_j^* \\ 0, & \text{if } c_j^*(n,m) < t_j^* \end{cases}, \quad * = H,V,D. \tag{3.18}$$

Then $\bar{w}_j^*$ is called the associated wavelet coefficients matrix (AWCM) of IDCM $\bar{c}_j^*$. Instead of computing the total power of w_j^*, we define the signature of energy (SE) as

$$\bar{e}_j^* = \frac{1}{L_j}\sum_{n=1}^{N}\sum_{m=1}^{M}(\bar{w}_j^*(n,m))^2. \tag{3.19}$$

Like w_j^*, $\bar{w}_j^*$ is also nearly zero-mean, so SE $\bar{e}_j^*$ is approximately the variance of the nonzero elements in $\bar{w}_j^*$. $\bar{e}_j^*$ more accurately reflects the variation of the interested structures than does e_j^* as defined in (3.17).

$$\vec{p}_j^{\,D}(k) = \begin{cases} \sum_{m=1}^{k} \bar{c}_j^D(N-k+m,m), & k = 1,2,\ldots,N \\ \sum_{m=k-N+1}^{k} \bar{c}_j^D(N-k+m,m), & k = N+1,\ldots,M \\ \sum_{m=k-N+1}^{M} \bar{c}_j^D(N-k+m,m), & k = M+1,\ldots,K \end{cases} \tag{3.13}$$

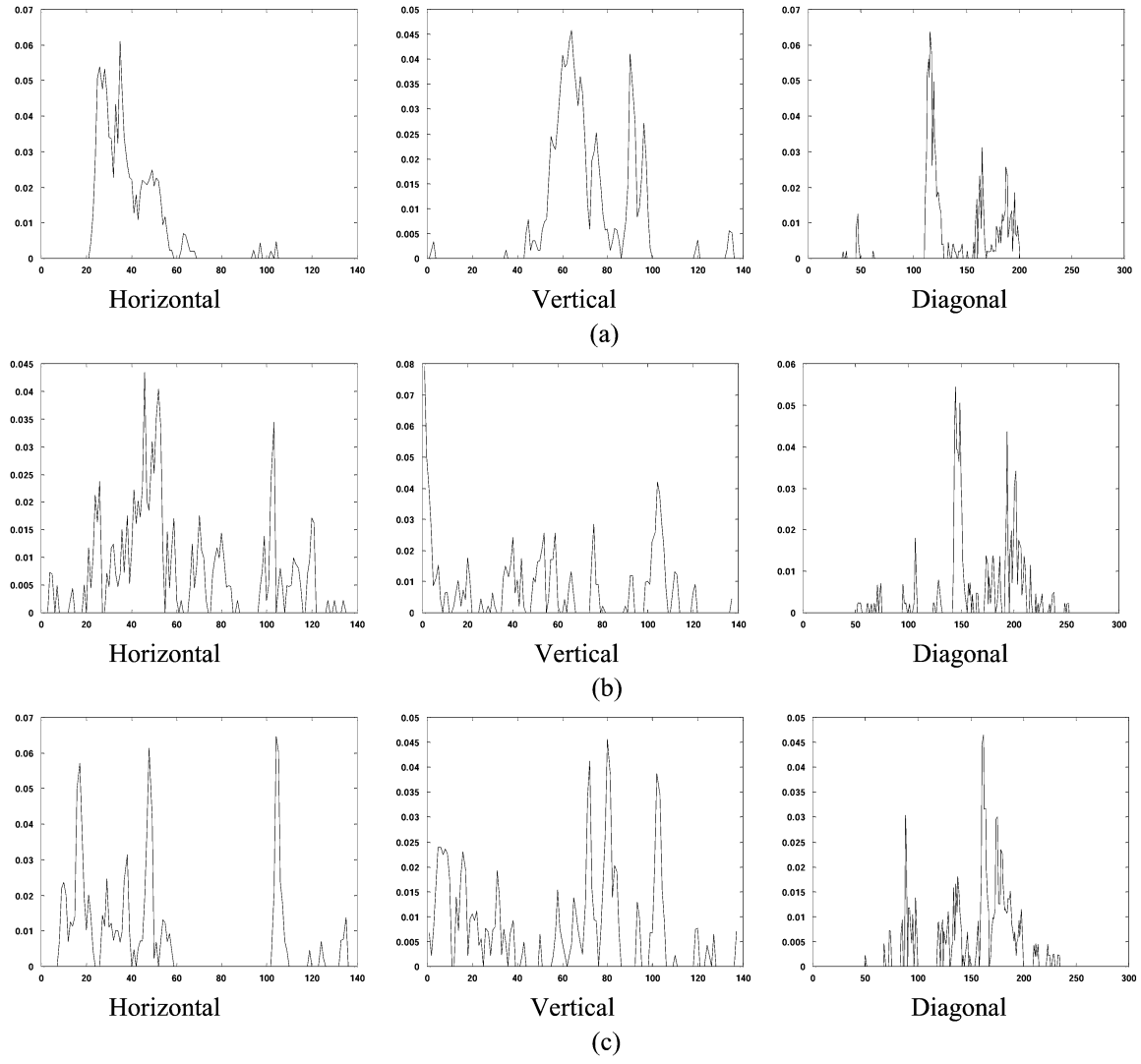

Fig. 8. The NAPV of the ICDMs in Fig. 7. The horizontal, vertical, and diagonal NAPVs for (a) palmprint 1, (b) palmprint 2, and (c) palmprint 3.

IV. Experiments

A. The Identification Strategy

Table I summarizes the context-based statistical signatures defined in the last section. Suppose the palmprint images are decomposed into J wavelet scales. Each palmprint image would have three pairs of SGAC signatures, $3 \cdot J$ SD signatures, $3 \cdot J$ SSD signatures and $3 \cdot J$ SE signatures. These statistical signatures can approximately describe a palmprint accurately and then can be used to uniquely identify a person. Compared with the line segments or interesting points based palmprint verification schemes, the proposed approach is particularly lower in the data storage. In pattern recognition, it is often expected that the database can be grouped into several classes for faster retrieval or other analytical purposes. These statistical signatures can also provide a classification scheme of palmprints conveniently. The flowchart in Fig. 9 illustrates the classification and identification scheme used in this paper. The SAGC signatures are employed to group the palmprints in the database into several classes. (In the experiments of next subsection, 50 palmprints were classified into eight classes using SAGC signatures.) When the database is growing large, the SE signatures can be used for more detailed classification. Once an input palmprint is identified as belonging to a class, it is matched with all the palmprints in that class to determine if it is among them.

Since different signatures have different metrical units, so their compared errors could not be added up directly. We computed the relative errors in the identification process. For expression convenience, we denote by Θ_1 the vector containing all the SAGC signatures over directions, and by Θ_2 the vector containing all the SD signatures over scales and directions, and by Θ_3 and Θ_4 those for SSD and SE signatures respectively. Denote by $\Theta_i^k, i = 1, 2, \ldots, 4$, these vectors of the kth palmprint in the database. The total relative error (TRE) of an input Θ_i with the stored Θ_i^k, denoted by $E_{r,(i)}^k$, is computed as

$$E_{r,(i)}^k = \sum_l \left| \frac{\Theta_i(l) - \Theta_i^k(l)}{\Theta_i^k(l)} \right|. \tag{4.1}$$

TABLE I
SUMMARY OF THE WAVELET SIGNATURES DEFINED FOR A PALMPRINT, WHERE J IS THE TOTAL DECOMPOSITION SCALE OF THE WT

Signature	Total number	Description
Signature of average gravity center (SAGC)	3 pairs	The average of the gravity centers of the interested directional context matrices (IDCM) over all scales. They measure the global position of the interested structures of principle lines and heavy wrinkles in a palmprint.
Signature of density (SD)	$3J$	The average number of the nonzero elements that exist in the square window centered at a nonzero element in an IDCM. They measure the compactness of the points in an IDCM.
Signature of spatial disperse (SSD)	$3J$	The reciprocal of the standard deviation of the normalized associated projection vector (NAPV) of an IDCM. They measure the spatial distribution of an IDCM in the corresponding direction.
Signature of energy (SE)	$3J$	The mean energy of the nonzero elements in the associated wavelet coefficients matrix (AWCM) of an IDCM. An SE measures the variance of the interested structures in an AWCM, and a sequence of SEs reflects the distribution of energy along the frequency axis over wavelet scales.

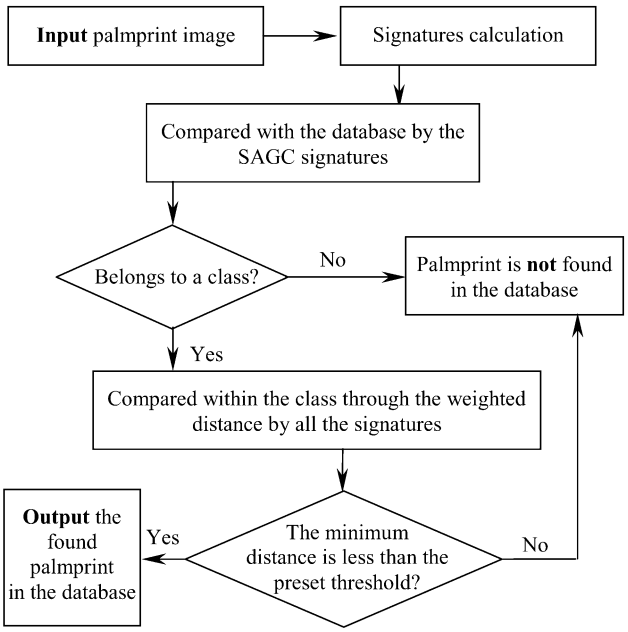

Fig. 9. Identification strategy of the input palmprint.

The WD between the input palmprint and the kth palmprint in the class is calculated by using the TREs of each kind of signature

$$D_w^k = \sum_{i=1}^{4} \lambda_i E_{r,(i)}^k \tag{4.2}$$

where $\{\lambda_i\}_{i=1,2,...,4}$ is a preset weight sequence, which is determined by the reliability and stability of the signatures. In our experience, the SGAC and SE signatures are more reliable and stable than the SD and SSD signatures. It is appropriate to assign SGAC and SE with a greater weight than SD and SSD. Particularly, by normalizing λ_1 and λ_4 to be 1, λ_2 and λ_3 can be set around 0.6. The experimental results are insensitive to the variations of λ_2 and λ_3.

Denote

$$D_w = \min_{k=1,2,...} D_w^k. \tag{4.3}$$

If $D_w \leq \mathrm{T}$, where T is the preset threshold, the input palmprint is verified as the one whose WD from the input palmprint is equal to D_w. Otherwise, the input palmprint is judged as being out of the database.

The preset T is determined as follows. If the input palmprint is in the database, its relative error with the same person's palmprint in the database is assumed to be less than 10% with respect to each signature. T can thus be calculated by summing up all the relative errors, which are supposed to be 0.1, taking the weighted value into consideration. Since there are six SAGC signatures and $3 \cdot J$ SD, SSD, and SE signatures, we have

$$T = 0.1 \cdot \left(\lambda_1 \cdot 6 + 3J \cdot \sum_{i=2}^{4} \lambda_i \right). \tag{4.4}$$

It is well known that in the pattern recognition a low threshold T produces a low false-identification rate (FIR) but a high false-rejection rate (FRR), while a high threshold T produces a low FRR but a high FIR. T is thus a tradeoff between FIR and FRR. Interestingly, the experiments in the next subsection demonstrate that the presented scheme works particularly well at reducing the FIR even when T is high. In practice, it is possible to assign a value to T that produces a low FRR yet nonetheless maintains a low FIR.

B. Experimental Results

We captured 200 palmprint samples from 50 persons. Four samples were captured for each person, at different times by CCD at resolution 65 dpi. Of the 200 palmprints, 50 samples were used to form the database and the other 150 samples were used for performing the identification experiments. The size of the palmprint images after preprocessing is 150×150 and the wavelet employed in the experiments is biorthogonal wavelet CDF(1, 3) constructed in [15]. The constant L [referring to (3.5)] is set as 200.

The 50 persons were grouped into eight classes using the SAGC signatures. The distribution of the 50 pairs of SAGCs in Euclidean space is shown in Fig. 10 (the total wavelet decomposition scale is set as $J = 3$). In the horizontal, vertical, and diagonal directions, the palmprints were divided into two categories according to the positions of their gravity centers (the two categories should have some overlap near the boundary, which is illustrated in Fig. 10). Finally, the 50 palmprints were classified into $2^3 = 8$ classes. Table II lists the number of palmprints

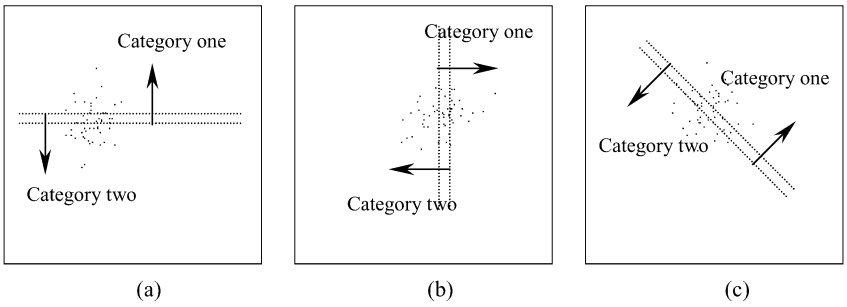

Fig. 10. The spatial distribution of the signatures of average gravity center (SAGC) of the 50 palmprints in our database. (a) Horizontal direction. (b) Vertical direction. (c) Diagonal direction. For each of the three directions, the palmprints are divided into two categories, which have some overlap near the boundary. Finally, the 50 palmprints are classified into eight classes, and the number of palmprints in each class is listed in Table II.

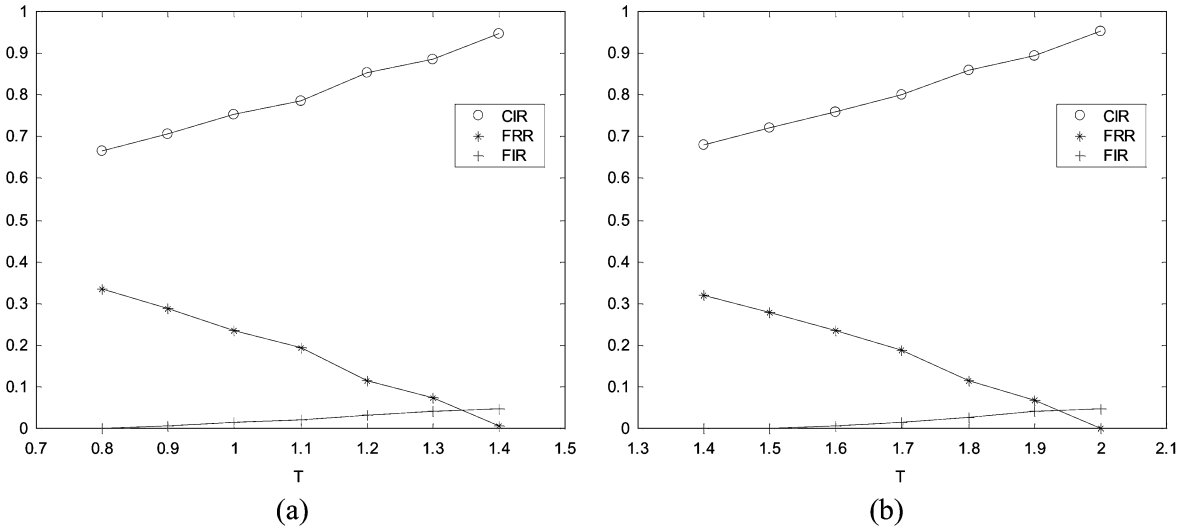

Fig. 11. Experimental results when wavelet decomposition scale is $J = 2$. (a) With weight sequence $\{\lambda_i\} = \{1, 0, 0, 1\}$; (b) With weight sequence $\{\lambda_i\} = \{1, 0.6, 0.6, 1\}$.

in each class. The total number of palmprints is greater than 50 because there are some overlaps across some classes.

After an input palmprint is adjudged to belong to a class, it is compared with all the palmprints in the class by computing WD in order to determine if it is among them. Figs. 11 and 12 illustrate the experimental results of the proposed scheme using different wavelet decomposition scales and weight sequences. We plotted the curves of corrected identification rate (CIR), FIR, and FRR versus threshold T. Since the wavelet energy signatures [referring to (3.17)] have been successfully used in texture analysis [27]–[31] applications such as fingerprint recognition [32], we plotted in Fig. 13 the palmprint identification results only using the energy signatures. The identification strategy is similar to that in Section IV-A.

Fig. 13 shows that the palmprint identification result was not satisfied using only the energy signatures. The CIR is not sufficiently high and the FIR is high when increasing the threshold. Figs. 11 and 12 show that the proposed scheme gives much better results. Particularly, it has a very low FIR, even when the threshold T is high. That is to say, we could assign a proper value with T to suppress FRR without worrying about FIR increasing too much. It is also observed that the proposed method still produces acceptable results when a small wavelet decomposition number is used. In contrast with $J = 3$, the CIR, FIR, and FRR results degenerate only slightly when $J = 2$. However, the identification results by only energy signatures are very poor when the total decomposition scale number J is small. This implies that the signatures of our scheme offer a good characterization of palmprint features. In Figs. 11(a) and 12(a), the weights λ_2 and λ_3 were set as 0.6, and in Fig. 11(b) and 12(b) they were set as 0, i.e., SD and SSD were not used in identification. We can see that although SAGC and SE signatures lead to good results, SD and SSD signatures are very helpful in improving the identification accuracy.

TABLE II
NUMBER OF PALMPRINTS OF THE EIGHT CLASSES GROUPED BY SAGC SIGNATURES

Class	1	2	3	4	5	6	7	8
number	5	14	13	4	6	15	10	3

Table III lists the palmprint identification results reported in the line-segment matching and half interesting-point matching methods of papers [4] and [6]. It should be noted that in those line or point based methods [4]–[6], the palmprint images are first inked in a paper, and then the paper palmprints are scanned

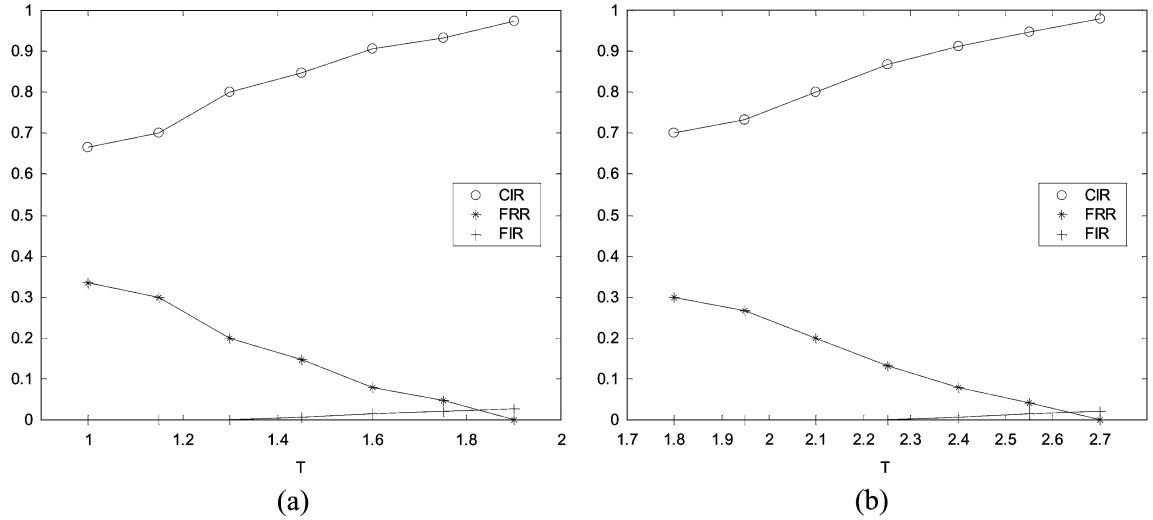

Fig. 12. Experimental results when wavelet decomposition scale is $J = 3$. (a) With weight sequence $\{\lambda_i\} = \{1, 0, 0, 1\}$. (b) With weight sequence $\{\lambda_i\} = \{1, 0.6, 0.6, 1\}$.

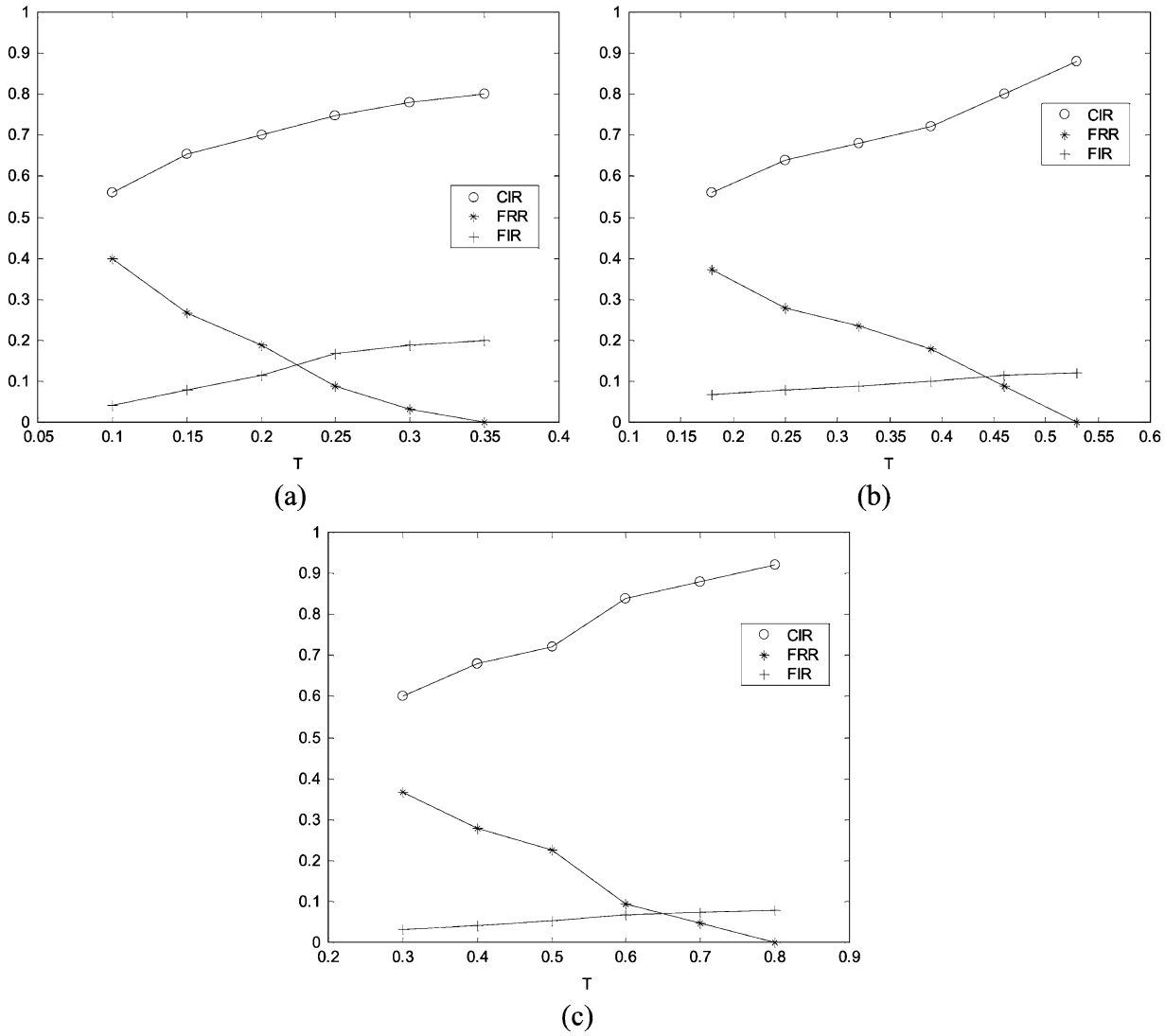

Fig. 13. Experimental results by the traditional wavelet energy signatures. (a) With wavelet decomposition scale $J = 2$. (b) With wavelet decomposition scale $J = 3$. (c) With wavelet decomposition scale $J = 4$.

by a scanner. They are basically designed for off-line analysis. In [4], 60 palmprints, which were collected by scanning at a resolution of 100 dpi, were used for experiments. In [6], 200 palmprints were collected from 100 persons by scanning at a

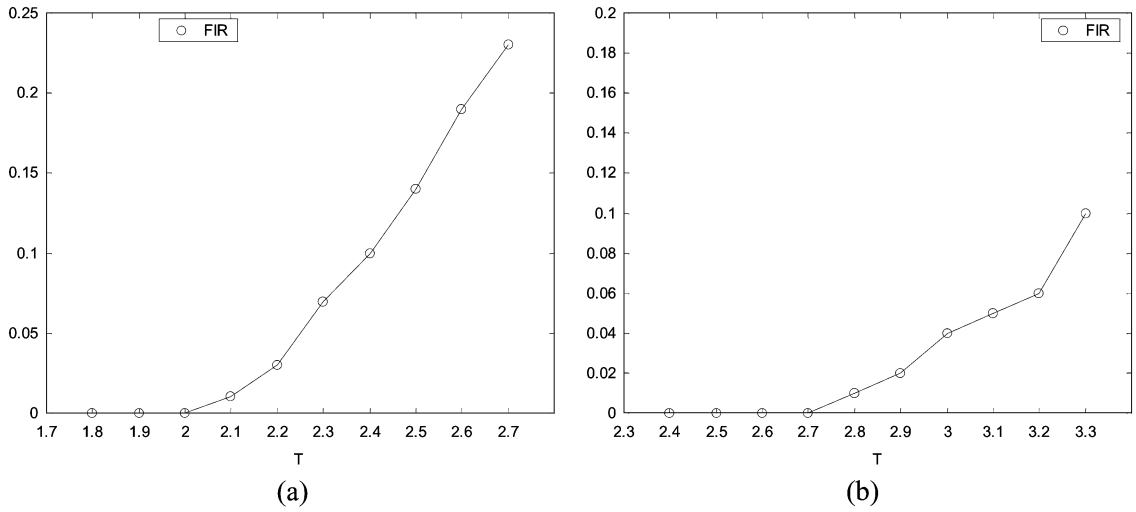

Fig. 14. Performance of the proposed method at rejecting the palmprints not in the database. (a) FIR versus threshold T when $J = 2$. (b) FIR versus threshold T when $J = 3$. It is seen that the FIR is very low when T is around the value computed by (4.4).

TABLE III
PALMPRINT IDENTIFICATION RESULTS OF PAPERS [4] AND [6], IN WHICH THE METHODS ARE LINE-SEGMENT MATCHING AND HALF INTERESTING-POINT MATCHING BASED, AND THE PROPOSED METHOD

Methods	CIR	FIR	FRR
In [4]	93.3%	--	--
In [6]	95%	--	--
Proposed	98%	2%	0%

resolution of 125 dpi. (In point matching method [5], 30 palmprints of three persons were collected and the scanning resolution is 200 dpi. The point extraction and matching performance was analyzed but the CIR result was not shown in that paper.) The palmprints used in this paper were captured with a CCD at a resolution of 65 dpi. The result of the proposed method listed in Table III is obtained subject to the conditions that $J = 3, \{\lambda_i\} = \{1, 0.6, 0.6, 1\}$ and $T = 2.7$. Unlike the schemes in [4]–[6], the proposed scheme is intended to allow on-line access control. The implementation speed is reasonable. The whole identification process of an input palmprint can be completed within 3 s by running our nonoptimized Matlab code in the PC of Intel P4 1.7-GHZ CPU and 512-MB RAM. The speed will be much faster when we embed the algorithm into the real system by C code. One of the problems in line- or point-based methods is the disturbance of redundant wrinkle and crease features in determining the line segments and interesting points of principal lines. The proposed statistical signatures are global measurements of the palmprint image, and they are more robust to noise and the variations of minor features.

To test how well the proposed method rejects the palmprints not in the database, we compared each one of the 50 persons' palmprints with the other 49 persons' palmprints, seeking false identifications. We performed the experiments with total wavelet decomposition scale number $J = 2$ and $J = 3$. The weights were $\{\lambda_i\} = \{1, 0.6, 0.6, 1\}$. Since the threshold calculated with (4.4) is $T = 1.92$ for $J = 2$ and $T = 2.58$ for $J = 3$, we carried out the experiments by taking T in interval $[1.8, 2.7]$ for $J = 2$ and interval [2.4, 3.3] for $J = 3$. Generally, the FIR is low when threshold T is small and it increases with as T increases. Fig. 14 compares the curves of FIR versus T. The FIR is very low when T is around the value calculated by (4.4). This result shows that the proposed method is able to reject palmprints not in the database.

V. CONCLUSION

This paper presents a statistical approach to palmprint identification that uses low-resolution images. We transform the palmprints into the wavelet domain and then identify the predominant structures using context modeling according to the appearances of the principal lines in each subband. By using the interested context image, we characterize an input palmprint with a set of statistical signatures. Some of the signatures are used to classify the palmprints, and all the signatures are used to calculate the WDs between the palmprints and the database. The proposed scheme provides an adequate statistical description of the principal lines and heavy wrinkles, which convey considerable information for purposes of individual identification. The experiments were performed using two hundreds palmprint images from fifty persons. The 50 individuals were classified into eight categories. The corrected recognition rate was as high as 98%. The proposed scheme works very well at suppressing the false identification rate and robust to the threshold. These results are encouraging and the scheme will be tested on a much larger database. The main limitation of the approach is that the used signatures are global measurements, and the signatures of some palmprints are very similar. It is to be hoped that some local signatures (that is to say, the signatures are computed at different spatial locations of the palmprint) can be defined in the future work to identify the highly similar palmprints.

REFERENCES

[1] B. Miller, "Vital signs of identity," *IEEE Spectrum*, vol. 32, pp. 22–30, Feb. 1994.
[2] A. K. Jain, R. Bolle, and S. Pankanti, Eds., *Biometrics: Personal Identification in Networked Society*. Norwell, MA: Kluwer, 1999.

[3] D. Zhang, *Automated Biometrics—Technologies and Systems*, A. K. Jain, Ed. Norwell, MA: Kluwer, 2000.
[4] D. Zhang and W. Shu, "Two novel characteristics in Palmprint verification: Datum point invariance and line feature matching," *Pattern Recognit.*, vol. 32, pp. 691–702, 1999.
[5] N. Duta, A. K. Jain, and K. V. Mardia, "Matching of palmprints," *Pattern Recognit. Lett.*, vol. 23, pp. 477–485, Apr. 2002.
[6] J. You, W. Li, and D. Zhang, "Hierarchical pamlprint identification via multiple feature extraction," *Pattern Recognit.*, vol. 35, pp. 847–859, Apr. 2002.
[7] W. K. Kong and D. Zhang, "Palmprint texture analysis based on low-resolution images for personal identification," in *Proc. ICPR 2002*, QC, Canada, pp. 807–810.
[8] J. Chen, C. Zhang, and G. Rong, "Palmprint recognition using crease," in *Proc. Int. Conf. Image Processing*, Oct. 2001, pp. 234–237.
[9] A. K. Jain, L. Hong, S. Pankanti, and R. Bolle, "An identity-authentication system using fingerprints," *Proc. IEEE*, vol. 85, pp. 1365–1388, Sept. 1997.
[10] A. K. Jain, S. Prabhakar, and L. Hong, "A multichannel approach to fingerprint classification," *IEEE Trans. Pattern Anal. Machine Intell.*, vol. 21, pp. 348–359, Apr. 1999.
[11] R. Sanchez-Reillo, C. Sanchez-Avila, and A. Gonzalez-Marcos, "Biometric identification through hand geometry measurements," *IEEE Trans. Pattern Anal. Machine Intell.*, vol. 22, pp. 1168–1171, Oct. 2000.
[12] R. Zunkel, "Hand geometry based authentication," in *Biometrics: Personal Identification in Networked Society*, A. Jain, R. Bolle, and S. Pankanti, Eds. Norwell, MA: Kluwer, 1999.
[13] R. P. Wildes, "Iris recognition: An emerging biometric technology," *Proc. IEEE*, vol. 85, pp. 1348–1363, Sept. 1997.
[14] W. Chou, "Discriminant-function-based minimum recognition error rate pattern-recognition approach to speech recognition," *Proc. IEEE*, vol. 88, pp. 1201–1223, Aug. 2000.
[15] C. Liu and H. Wechsler, "A shape- and texture-based enhanced Fisher classifier for face recognition," *IEEE Trans. Image Processing*, vol. 10, pp. 598–608, Apr. 2001.
[16] I. Daubechies, *Ten Lectures on Wavelets*. Philadelphia, PA: SIAM, 1992.
[17] S. Mallat, "A theory for multiresolution signal decomposition: The wavelet representation," *IEEE Trans. Pattern Anal. Machine Intell.*, vol. 11, pp. 674–693, July 1989.
[18] S. Mallat and S. Zhong, "Characterization of signals from multiscale edges," *IEEE Trans. Pattern Anal. Machine Intell.*, vol. 14, pp. 710–732, July 1992.
[19] M. Vetterli and C. Herley, "Wavelet and filter banks: Theory and design," *IEEE Trans. Signal Processing*, vol. 40, pp. 2207–2232, Sept. 1992.
[20] S. G. Chang, B. Yu, and M. Vetterli, "Spatially adaptive wavelet thresholding with context modeling for image denoising," *IEEE Trans. Image Processing*, vol. 9, pp. 1522–1531, Sept. 2000.
[21] X. Wu, "Lossless Compression of continuous-tone images via context selection, quantization, and modeling," *IEEE Trans. Image Processing*, vol. 6, pp. 656–664, May 1997.
[22] Y. Yoo, A. Ortega, and B. Yu, "Image subband coding using context-based classification and adaptive quantization," *IEEE Trans. Image Processing*, vol. 8, pp. 1702–1715, Dec. 1999.
[23] J. Liu and P. Moulin, "Information-theoretic analysis of interscale and intrascale dependencies between image wavelet coefficients," *IEEE Trans. Image Processing*, vol. 10, pp. 1647–1658, Nov. 2001.
[24] R. R. Coifman and D. L. Donoho, "Translation-invariant de-noising," in *Wavelet and Statistics*, A. Antoniadis and G. Oppenheim, Eds, Berlin, Germany: Springer-Verlag, 1995.
[25] J. M. Shapiro, "Embedded image coding using zerostrees of wavelet coefficients," *IEEE Trans. Signal Processing*, vol. 41, pp. 3445–3462, Dec. 1993.
[26] A. K. Jain, R. P. W. Duin, and J. Mao, "Statistical pattern recognition: A review," *IEEE Trans. Pattern Anal. Machine Intell.*, vol. 22, pp. 4–37, Jan. 2000.
[27] T. Chang and C.-C. J. Kuo, "Texture analysis and classification with tree-structured wavelet transform," *IEEE Trans. Image Processing*, vol. 2, pp. 429–441, Oct. 1993.
[28] S. Pittner and S. V. Kamarthi, "Feature extration from wavelet coefficients for pattern recognition tasks," *IEEE Trans. Pattern Anal. Machine Intell.*, vol. 21, pp. 83–88, Jan. 1999.
[29] A. Laine and J. Fan, "Texture classification by wavelet packet signitures," *IEEE Trans. Pattern Anal. Machine Intell.*, vol. 15, pp. 1186–1191, Nov. 1993.
[30] M. Unser, "Texture classification and segmentation using wavelet frames," *IEEE Trans. Image Processing*, vol. 4, pp. 1549–1560, Nov. 1995.
[31] G. V. de Wouwer, P. Scheunders, and D. V. Dyck, "Statistical texture characterization from discrete wavelet representation," *IEEE Trans. Image Processing*, vol. 8, pp. 592–598, Apr. 1999.
[32] M. Tico, P. Kuosmanen, and J. Saarinen, "Wavelet domain features for fingerprint recognition," *Electron. Lett.*, vol. 37, pp. 21–22, Jan. 2001.

Lei Zhang received the B.S. degree in 1995 from Shenyang Institute of Aeronautic Engineering, Shenyang, China, and the M.S. and Ph.D. degrees in electrical and engineering from Northwestern Polytechnical University, Xi'an, China, in 1998 and 2001, respectively.

From 2001 to 2002, he was a Research Associate in the Department of Computing, The Hong Kong Polytechnic University, Kowloon. Currently, he is a Postdoctoral Researcher in the Department of Electrical and Computer Engineering, McMaster University, Hamilton, ON, Canada. His research interests include digital signal and image processing, pattern recognition, optimal estimation theory, and wavelet transforms.

David Zhang graduated in computer science from Peking University, Peking, China, in 1974. He received the M.Sc. and Ph.D. degrees in computer science and engineering from the Harbin Institute of Technology (HIT), Harbin, China, in 1983 and 1985, respectively. In 1994, he received the Ph.D. degree in electrical and computer engineering from the University of Waterloo, ON, Canada.

From 1986 to 1988, he was a Postdoctoral Fellow at Tsinghua University and then became an Associate Professor at Academia Sinica, Beijing, China. Currently, he is a Professor with the Hong Kong Polytechnic University, Kowloon. He is Founder and Director of the Biometrics Technology Centre supported by the Government of the Hong Kong SAR (UGC/CRC). He is also an Adjunct Professor at Tsinghua University, Shanghai Jiao Tong University, Harbin Institute of Technology, and the University of Waterloo. His research interests include automated biometrics-based authentication, pattern recognition, and biometric technology and systems. He has published over 120 journal papers, 20 book chapters, and nine books.

Dr. Zhang is an Associate Editor for over ten international journals, including the IEEE TRANSACTIONS ON SYSTEMS, MAN, AND CYBERNETICS (Parts A and C) and the IEEE TRANSACTIONS ON PATTERN RECOGNITION. He is Founder and Editor-in-Chief of the *International Journal of Image and Graphics (IJIG)*, Book Editor for the *Kluwer International Series on Biometrics (KISB)*, and Program Chair for the First International Conference on Biometrics Authentication (ICBA). He has received several awards since 1980 for his work on biometrics projects.